

RESEARCH

Open Access



Effect of cationic monomer structure on the aggregation behavior of amphoteric acrylic polymer around isoelectric point

Qijun Li¹, Yudan Yi², Ya-nan Wang^{1,2*} , Jing Li³ and Bi Shi^{1,2}

Abstract

Amphoteric polymer can be used as retanning agent in leather manufacture. It is particularly useful in chrome-free tanning systems since it can regulate the charge properties of chrome-free leather and enhance the fixation of anionic post-tanning chemicals in leather. However, the aggregation and precipitation of amphoteric polymer retanning agents around the isoelectric point (pI) hinder their wide application. Herein, we synthesized five amphoteric acrylic polymers (AAPs) by free radical copolymerization with acrylic acid and five different cationic acrylic monomers. The effect of cationic monomer structure on the aggregation behavior of AAPs was investigated. The aggregation of AAPs in aqueous solution showed pH and concentration dependence. Light scattering analysis showed that Poly (AA-co-MAPTAC) and Poly (AA-co-DMAPMA) were in the shape of coiled linear flexible chains with small particle size (R_g 7.6 nm and 14.8 nm, respectively) near the pI. However, Poly (AA-co-DAC), Poly (AA-co-DMC) and Poly (AA-co-DMAEMA) were in the shape of hollow spheres and exhibited serious aggregation. Quantum chemical calculations suggested that the amide groups in the cationic monomers MAPTAC and DMAPMA enhanced the nucleophilicity of AAPs. Thus the corresponding AAPs could carry a large number of cationic charges to slow their aggregation when the pH just climbed over the pI. The results are expected to provide theoretical reference for the synthesis and wide-spread application of AAPs.

Keywords: Amphoteric acrylic polymer, Isoelectric point, Aggregation behavior, Cationic monomer, Retanning

1 Introduction

Chrome-free tanning technology can eliminate the emission of chrome-containing wastewaters and solid wastes from the source, and play an important role in promoting the sustainable development of the leather industry [1–3]. In recent years, significant progress has been achieved in the tanning technology of chrome-free leather manufacturing system [4, 5]. However, the conventional post-tanning chemicals and technologies are not well compatible with this system. In particular, the isoelectric point (pI) of chrome-free tanned semi-finished leather

(wet white) is significantly different from that of chrome tanned one [6], which leads to poor fixation of conventional anionic post-tanning chemicals in the chrome-free leather [7]. It has been reported that amphoteric polymer retanning agents with appropriate pI could adjust the charge properties of wet white leather to improve penetration and fixation of post-tanning chemicals, so as to result in satisfactory physical and organoleptic properties of chrome-free leathers [8–10].

According to structures, amphoteric polymer retanning agents are classified into amphoteric acrylic polymer [11–13], amphoteric polyurethane [14, 15], amphoteric syntan [16], etc. Among them, amphoteric acrylic polymer (AAP), which is a linear polymer synthesized by free radical co-polymerization of anionic acrylic monomers and cationic acrylic monomers, is

*Correspondence: wangyanan@scu.edu.cn

¹ Key Laboratory of Leather Chemistry and Engineering (Sichuan University), Ministry of Education, Chengdu 610065, China
Full list of author information is available at the end of the article

the most widely used type. During the retanning process, the pH of float drops from 5–6 at the beginning to below 4 at the end. This pH change usually passes through the pI of AAP. When the pH of float is close to the pI of AAP, the cationic and anionic groups on the AAP chains will strongly interact with each other through electrostatic force. This may lead to serious aggregation and precipitation of AAP [17], and then cause the uneven penetration and distribution of AAP in the leather.

In order to achieve wide application of AAP in chrome-free tanning system, it is necessary to develop new products with a certain dispersion stability near the pI. The selection of anionic/cationic acrylic monomers is one of the crucial issues. The protonation ability of AAPs at a certain pH differ from one another due to their different monomer structures, which will affect the strength of the intra-/inter-chain electrostatic interactions, as well as the spatial structure and aggregation state of AAPs [18–20]. In this study, five cationic acrylic monomers (Fig. 1) were selected to synthesize AAPs by free radical copolymerization with acrylic acid, respectively. The structures of the AAPs were characterized by Fourier transform infrared (FT-IR) spectroscopy, nuclear magnetic resonance (NMR) spectroscopy and size exclusion chromatography (SEC). The effect of chemical structure of cationic monomers on the properties of AAPs, especially the aggregation behavior near the pI, was investigated by dynamic/static light scattering (DLS/SLS), diffusing wave spectroscopy (DWS), zeta potential and quantum chemical calculations. We hope to select suitable cationic monomers and guide the preparation of amphoteric polymer retanning agents for chrome-free tanning system.

2 Experimental

2.1 Materials

Acryloyloxyethyl trimethyl ammonium chloride (DAC, 80 wt%), 3-(methacryloylaminoethyl) trimethylammonium chloride (MAPTAC, 50 wt%), dimethylaminoethyl methacrylate (DMAEMA, 99.5 wt%), and dimethylaminopropyl methacrylamide (DMAPMA, 98.5 wt%) were purchased from Feymer Technology Co., Ltd. (Jiangsu, China). Methacryloxyethyl trimethyl ammonium chloride (DMC, 75 wt%) and Poly (diallyldimethylammonium chloride) (PDDA, 20 wt%) were purchased from Aladdin Reagent Co., Ltd. (Shanghai, China). Acrylic acid (AA, 99 wt%) was provided by Sichuan Decision New Material Technology Co., Ltd. (Sichuan, China). Ammonium persulfate and sodium bisulfite were purchased from Chengdu Kelong Chemical Reagent Co., Ltd. (Sichuan, China). Poly (vinyl sulfate) potassium (PVSK, 0.0025 mol/L) was purchased from Wako Pure Chemical Industries, Ltd. (Japan). PEO standards were purchased from Agilent Technologies Co., Ltd. (USA). PEG standards were purchased from Tosoh Corporation (Japan).

2.2 Preparation of AAPs

Acrylic acid (0.4 mol) and a certain amount of deionized water were first added to a four-necked round-bottom flask (500 mL) equipped with a thermometer, a stirrer and two constant pressure funnels, and then sodium hydroxide solution (32 wt%) was slowly added dropwise under stirring to control the neutralization degree (the stoichiometric proportion of the neutralized acrylic acid) to 95%. Then 0.14 mol cationic monomer and a chain transfer agent (0.1%–0.3% of the weight of blend monomer) were added. The temperature was kept below 40 °C by partially immersing the flask in a cold-water bath.

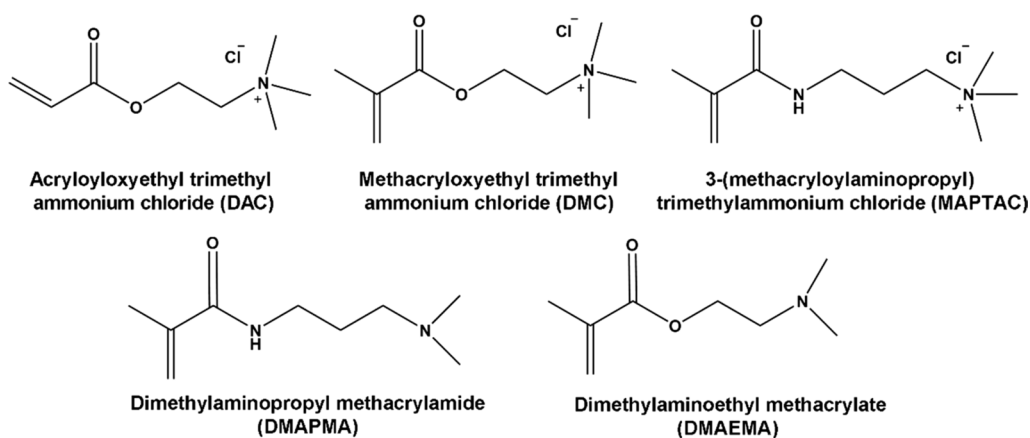


Fig. 1 Chemical structure of the cationic monomers

The theoretical solid content of the AAPs was controlled to 35% by adding deionized water into another empty reactor, and then the reactor was heated to 85 °C in an oil bath. Ammonium persulfate (1.5% of the weight of blend monomer) solution and the blend monomer solution were simultaneously added through constant flow pumps in 90 min. The temperature was kept constant for 120 min after feeding. Sodium bisulfite (1.5% of the weight of blend monomer) solution was added to remove the residual initiator. AAPs were obtained after cooling to room temperature.

2.3 FT-IR analysis

AAPs were lyophilized, ground to solid powder, and pressed using the KBr disk method. The FT-IR spectra of AAPs were recorded in the range from 400 to 4000 cm^{-1} using FT-IR spectrometer (Nicolet IS10, Thermo Fisher) with a resolution of 4 cm^{-1} and 64 scans.

2.4 ^{13}C NMR analysis

The lyophilized AAP was dissolved in D_2O to prepare a 200 mg/mL sample solution. The ^{13}C NMR spectra of AAPs were recorded on a NMR spectrometer (Avance II 400 MHz, Bruker).

2.5 SEC analysis

Weight-average molecular weight (M_w) and number-average weight (M_n) of AAPs were determined by SEC. Fifty μL of AAP solution (5 mg/mL) was filtrated through a membrane of 0.22 μm pore size. Then it was injected into the high-performance liquid chromatography (1260 Infinity II, Agilent) equipped with a TSK-gel GMPWXL column (7.8 mm \times 300 mm, Tosoh) and eluted by NaNO_3 (0.1 mol/L) at a flow rate of 0.6 mL/min under 30 °C. Molecular weight of the AAPs was calculated using The standard curve established by PEG and PEO standards.

2.6 Isoelectric point (pI) and particle size determination

The zeta potentials of AAP aqueous solution (5 mg/mL) in the pH range of 2.0–8.0 were determined using a particle size & zeta potential analyzer (NanoBrook Omni, Brookhaven). Each sample was tested 5 times at 25 °C to obtain the average. The pH value at the zero point of zeta potential was recorded as the pI of the AAP. The hydrodynamic diameter (D_h) and particle size distribution of AAP aqueous solution at different concentrations (0.5–5 mg/mL) or different pH (2.0–8.0) were also determined by this instrument. All the measurements were carried out at a scattering angle of 90° with an equilibration time of 3 min at 25 °C.

2.7 Turbidity measurement

The turbidity values of AAP aqueous solution (3 wt%) in the pH range of 2–8 were determined by a scattered light turbidimeter (WGZ-3, Xinrui). The test limit of this instrument is 1000 NTU.

2.8 DLS/SLS analysis

A series of AAP solutions (1.4–5.3 mg/mL) were prepared using citric acid-sodium citrate buffer (0.1 mol/L) of pH 4 as solvent. After filtration through membrane of 1.0 μm pore size, the samples were used for DLS/SLS measurements by a compact goniometer system (CGS-3, ALV) equipped with a He–Ne laser (wavelength $\lambda=632.8$ nm, 22 mW) at 25 °C. DLS measurement was carried out at a scattering angle of 90°, and the intensity correlation function $g^2(t)$ was analyzed using the Cumulant method to obtain the hydrodynamic radius (R_h) of the sample. SLS measurement was carried out at scattering angles from 40° to 140° with a step of 5°. The data were evaluated using Zimm plot extrapolation by ALV-Stat software to yield the radius of gyration (R_g) and second virial coefficient (A_2) of the sample.

2.9 DWS analysis

The intensity autocorrelation function of AAP aqueous solutions (5 mg/mL) at the pI was determined by DWS (DWS RheoLab, LS Instrument) with a laser at the wavelength of 685 nm (40 mW) using transmission mode. A cuvette with a thickness of 10 mm was used. The temperature was 25 °C, and the test time was 3 min.

2.10 Cationic degree determination

Cationic degree of AAPs, defined as the amount of substance of positive charge in the polymer per unit mass at a certain pH, was determined by the colloidal titration method [21, 22]. The pH of AAP solution (50 mL, 0.1 g/L) was adjusted to 2, 4, 6 and pI, and 15 mL PVS solution (0.0025 mol/L) was added. After stirring for 30 min, toluidine blue indicator was added. The blend was titrated with PDDA standard solution to the end point where the color changed from purple-red to blue, and precipitation was formed. Moreover, 50 mL deionized water was used for a blank determination. Each sample was tested in duplicate to obtain the average. The cationic degree was calculated as follows:

$$\text{Cationic degree (mmol/g)} = \frac{f \times (V_1 - V_2)}{m} \quad (1)$$

where f is the concentration of PDDA standard solution (0.005 mol/L), V_1 is the volume of PDDA solution used for blank titration (mL), V_2 is the volume of PDDA solution used for sample titration (mL), and m is the weight of the sample (g).

2.11 Quantum chemical calculations

The molecular models of AAPs with a polymerization degree of 3 (acrylic acid-cationic monomer-acrylic acid) were constructed. The density functional theory (DFT) method with B3LYP hybrid functional was used for computation, and the Gaussian basis set 6–31G(d) was chosen. All calculations were performed using Gaussian 09W program [23]. The optimized structures and harmonic vibrational properties of the models were obtained. The chemical potential μ and chemical hardness η were calculated from the highest occupied molecular orbital (HOMO) energy ε_H and the lowest unoccupied molecular orbital (LUMO) energy ε_L , and then the electrophilic factor ω was calculated using the following equations [24, 25]:

$$\mu = \frac{\varepsilon_H + \varepsilon_L}{2} \quad (2)$$

$$\eta = \varepsilon_H - \varepsilon_L \quad (3)$$

$$\omega = \frac{\mu^2}{2\eta} \quad (4)$$

3 Results and discussion

3.1 Structural characterization of AAPs

The FT-IR spectra of AAPs are shown in Additional file 1: Fig. S1. The ^{13}C -NMR spectra of AAPs are shown in Additional file 1: Fig. S2. The chemical shifts of secondary carbon atoms (C_j), tertiary carbon atoms (C_k) and quaternary carbon atoms (C_l) on the polymer backbone were observed at 35–38 ppm, 42–43 ppm and 44–45 ppm, respectively. These results demonstrated that AAPs were successfully synthesized [26]. Among the cationic monomers used for polymerization, DMC, DAC, and DMAEMA are acryloxy-alkyl cationic monomers with ester group in the side chain. MAPTAC and DMAPMA are acrylamide-alkyl cationic monomers with amide group in the side chain. Moreover, DMC, DAC, and MAPTAC are monomers with quaternary ammonium group. DMAPMA and DMAEMA are monomers with tertiary amine group. The structural features of the cationic monomers can also be characterized by FT-IR and ^{13}C -NMR spectra of AAPs (Additional file 1: Figs. S1, S2).

3.2 Molecular weight and pI of AAPs

Table 1 shows the M_w , M_n , polydispersity (M_w/M_n) and pI of AAPs. The molecular weights of AAPs were close (M_w between 64,000–72,000) by adjusting the amount of chain transfer agent during polymerization to better investigate the effect of cationic monomer structure on the properties of AAPs. The pIs of AAPs were between

Table 1 Molecular weight and pI of AAPs

Sample	M_w (g/mol)	M_n (g/mol)	M_w/M_n	pI
Poly (AA-co-DAC)	71,081	15,078	4.71	4.15
Poly (AA-co-DMC)	65,451	30,483	2.15	4.27
Poly (AA-co-MAPTAC)	62,734	13,396	4.68	4.33
Poly (AA-co-DMAPMA)	69,321	15,463	4.48	4.07
Poly (AA-co-DMAEMA)	64,491	29,555	2.18	3.95

3.9 and 4.4. Poly (AA-co-DMAPMA) and Poly (AA-co-DMAEMA) with tertiary amine group exhibited slightly lower pI than the polymers with quaternary ammonium group. Moreover, among the AAPs with quaternary ammonium group, the pI of Poly (AA-co-MAPTAC) containing amide in the cationic monomer was slightly higher than those of Poly (AA-co-DAC) and Poly (AA-co-DMC) containing ester.

3.3 Effect of pH on the aggregation behavior of AAPs

The pH dependence of the turbidity and the particle size distribution of AAP solutions are shown in Fig. 2. Each sample remained clear with very low turbidity at pH 2, 6 and 8. The D_h was as small as 10–20 nm. However, D_h and turbidity increased remarkably, and intense aggregation and even precipitation occurred when the pH was around 4, that is near the pI of AAPs (see Table 1). These results can be attributed to the classical pH-responsive property of amphoteric polyelectrolyte [27, 28]. When the pH was away from the pI, the polymer carried a large number of positive or negative net charges because of the protonation of cationic monomers or the dissociation of acrylic monomers. The polymer chains were unfolded and dispersed far from each other in aqueous media due to their electrostatic repulsion. When the pH was at the pI of AAPs, the polymer with zero net charge showed strong aggregation, possibly because the electrostatic attraction between/within the polymer chains was greater than the repulsion [29, 30].

Although the molecular weights of various AAPs were similar, Poly (AA-co-MAPTAC) and Poly (AA-co-DMAPMA) with amide in the cationic monomers had smaller D_h at the pI (800–1100 nm), whereas the other three AAPs with ester in the cationic monomers (D_h around 2000 nm) showed drastic aggregation and even precipitated at the pI. This phenomenon may be attributed to the different protonation ability of cationic monomers in different AAPs near the pI, which resulted in different strength of electrostatic interaction between polymer chains [31, 32]. Further analysis will be presented in the following sections.

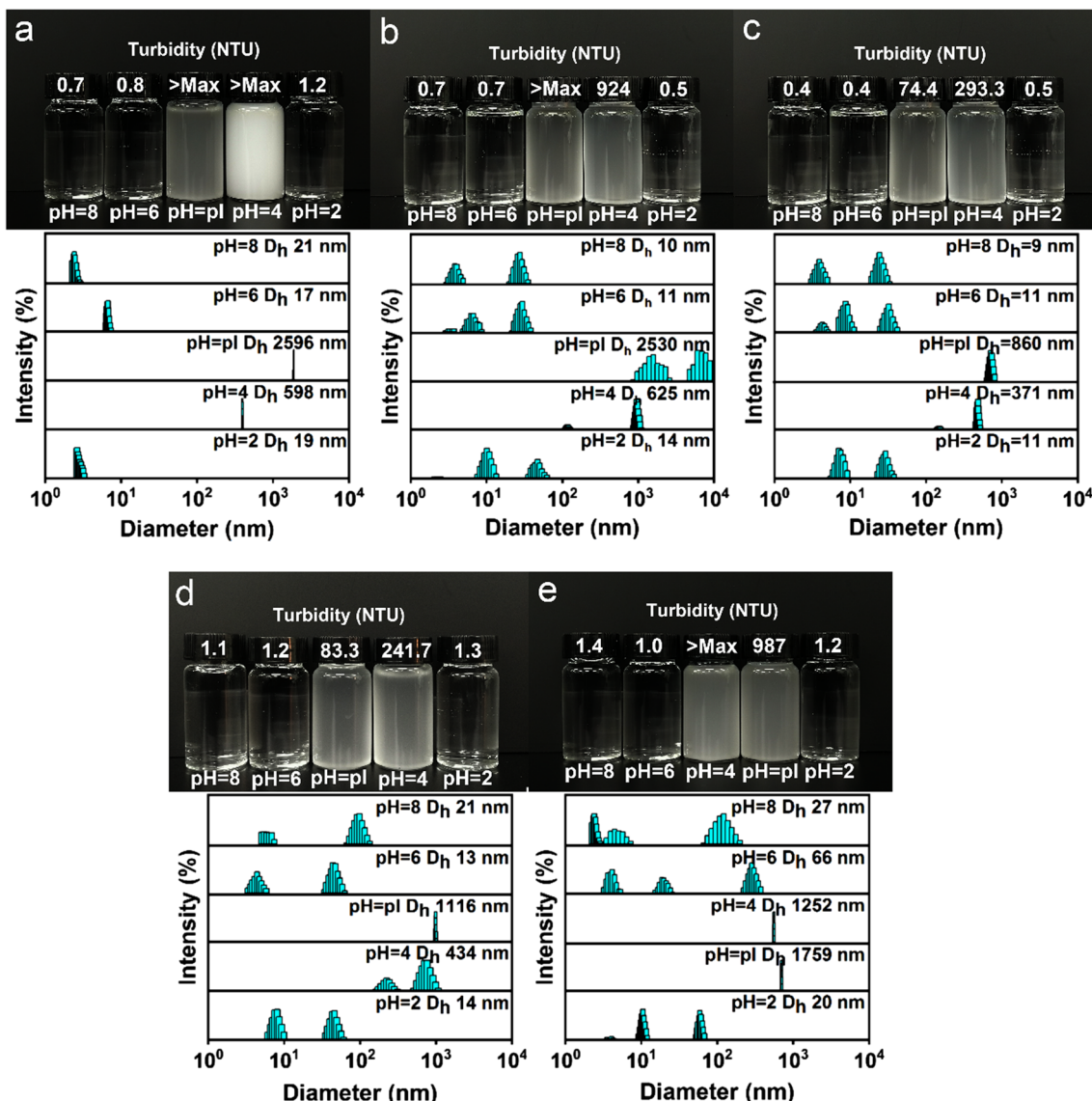


Fig. 2 Particle size distribution and turbidity of Poly (AA-co-DAC) (a), Poly (AA-co-DMC) (b), Poly (AA-co-MAPTAC) (c), Poly (AA-co-DMAPMA) (d) and Poly (AA-co-DMAEMA) (e) under different pH conditions

3.4 Effect of concentration on the aggregation behavior of AAPs

The aggregation behavior of AAPs showed concentration dependence in addition to pH dependence. As seen from Fig. 3, the D_h of AAPs at the pI increased with increased concentration because of the enhanced interactions between the polymer chains [33]. Similar to the pH dependence, AAPs with varied cationic monomer structures showed significant differences in the aggregation state at pI. When the concentration of AAP solution was 0.5 g/L, Poly (AA-co-MAPTAC) was the most stable with the smallest D_h (42 nm, Fig. 3c). When the concentration

increased to 5.0 g/L, the D_h of Poly (AA-co-MAPTAC) and Poly (AA-co-DMAPMA) that contained amide in the cationic monomers were around 1200 nm (Fig. 3c, d). The other AAPs containing ester in the cationic monomers exhibited serious aggregation at pI, and their D_h rose to more than 2000 nm.

3.5 DLS/SLS analysis

The conformations of AAPs in dilute solution near the pI (pH=4) were further analyzed by DLS/SLS. Table 2 shows that Poly (AA-co-DMAPMA) and Poly (AA-co-MAPTAC) had smaller R_g and R_h than the others. Their p

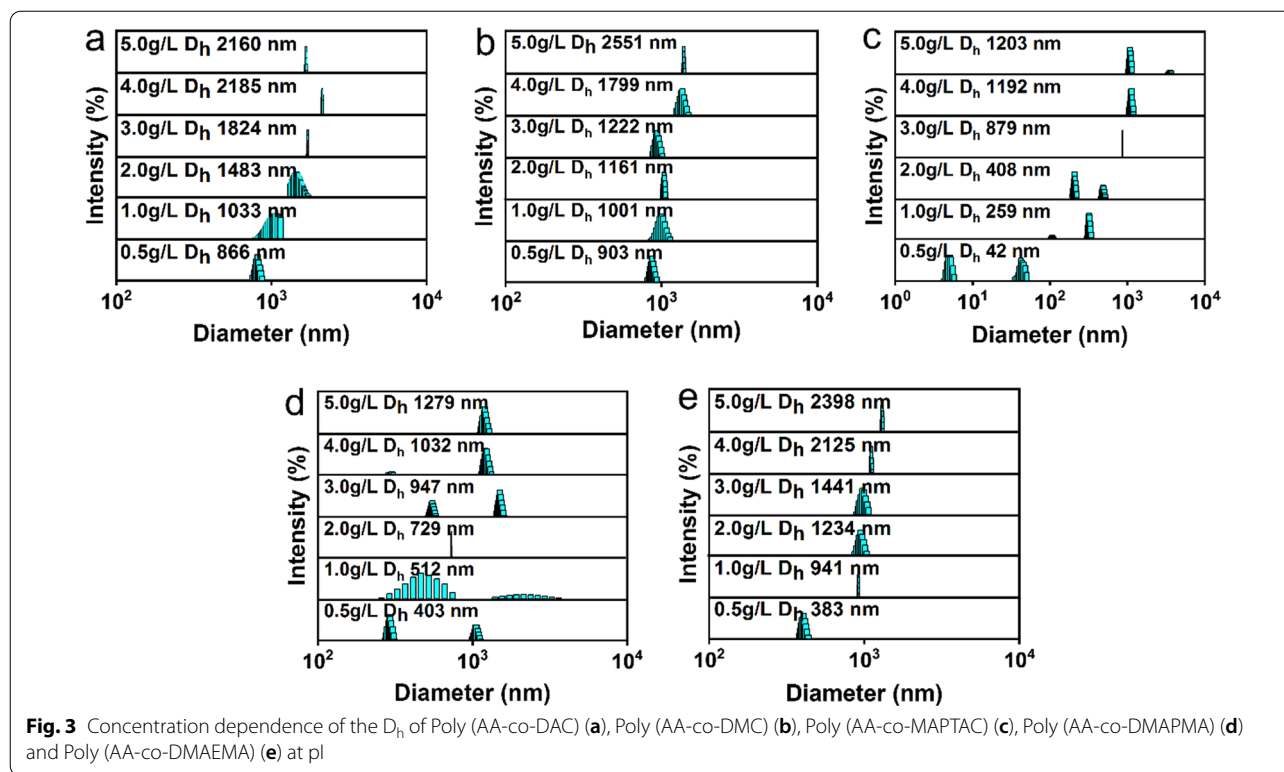


Table 2 Light Scattering Parameters of AAPs

Sample	R_g (nm)	R_h (nm)	ρ (R_g/R_h)	A_2 (mol·dm ³ /g ²)
Poly (AA-co-DAC)	241.8*	229.1	1.06	–
Poly (AA-co-DMC)	114.6*	122.4	0.94	–
Poly (AA-co-MAPTAC)	7.6	5.2	1.46	2.434e–06
Poly (AA-co-DMAPMA)	14.8	7.9	1.87	1.413e–06
Poly (AA-co-DMAEMA)	136.9	133.0	1.03	–1.211e–08

*Apparent radius of gyration

values (R_g/R_h) were 1.87 and 1.46, respectively, suggesting that they were in the shape of coiled linear flexible chains [34, 35]. The other three AAPs showed ρ values from 0.9 to 1.1, indicating that they were in the shape of hollow spheres and exhibited a higher extent of aggregation [36, 37]. Poly (AA-co-DMC) and Poly (AA-co-DAC) showed more intense aggregation behavior and obvious concentration dependence under this condition. Thus, their R_g and A_2 could not be obtained by Zimm plot extrapolation. A_2 was used to characterize the intensity of interactions between AAP chains in dilute solution. A_2 of Poly (AA-co-DMAEMA) was negative, suggesting that electrostatic attraction was dominant between the polymer chains, and Poly (AA-co-DMAEMA) tended to aggregate near the pI (pH=4). Conversely, A_2 was positive for Poly

(AA-co-DMAPMA) and Poly (AA-co-MAPTAC), which meant that electrostatic repulsion was dominant between the polymer chains, and the polymer tended to dissolve near the pI [37, 38]. Therefore, light-scattering analysis also demonstrated that Poly (AA-co-DMAPMA)/Poly (AA-co-MAPTAC) containing amide in the cationic monomer showed smaller size and more dispersed and flexible state in aqueous solution near the pI compared with the other AAPs containing ester in the cationic monomers.

3.6 DWS analysis

DWS, a modern light scattering technique, can be used to investigate the microrheological properties of polymer solution and to characterize turbid samples [39]. DWS extends DLS to media with multiple scattering, treating the transport of light as a diffusion process. It collects the multiply scattered light from the sample into a correlator, and the intensity autocorrelation function ($g^2(t) - 1$) can be determined to provide information about the local dynamics of particle dispersions [40].

The validity of the DWS is confirmed by the L/l^* , where L is the optical thickness of the cuvette, and l^* is the transport mean free path which represents the turbidity of sample. All DWS measurements were performed at $L/l^* > 4$ [41]. Figure 4 shows the intensity autocorrelation function of the AAPs at the pI. The correlation function

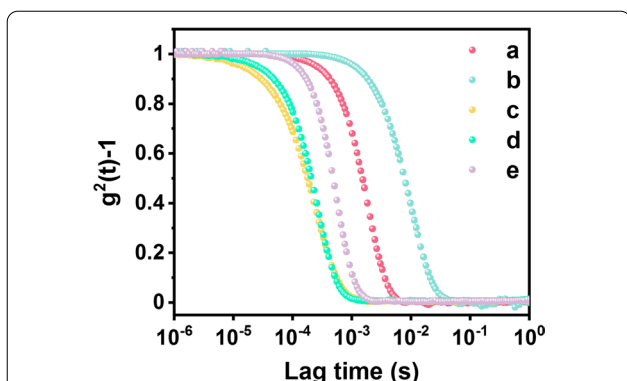


Fig. 4 Intensity autocorrelation function of Poly (AA-co-DAC) (a), Poly (AA-co-DMC) (b), Poly (AA-co-MAPTAC) (c), Poly (AA-co-DMAPMA) (d) and Poly (AA-co-DMAEMA) (e) at pI

of Poly (AA-co-DMC) decayed more slowly than the others. This fact demonstrated that Poly (AA-co-DMC) aggregated more heavily at the pI, resulting in a slower diffusion of polymer molecules in solution [42]. The correlation functions of Poly (AA-co-MAPTAC) and Poly (AA-co-DMAPMA) decayed faster among the AAPs, implying that they were more stable in solution. The DWS results were consistent with those of pH dependence and concentration dependence the AAPs.

3.7 Analysis on the charge-carrying ability of AAPs

The aggregation state of a polymer in solution is influenced by its charge density and charge distribution. In this study, the anionic monomer of the five AAPs was acrylic acid, while the cationic monomers differed from one another. The cationic degrees of these AAPs from pH 2 to 6 were determined to characterize the amount of cationic charge on the polymers (mmol/g). When the pH was near the pI (pH = pI and pH = 4), Poly (AA-co-MAPTAC) and Poly (AA-co-DMAPMA) showed higher cationic degrees than the others (Fig. 5). Moreover,

Table 3 Zeta potentials of AAPs near the pI

Sample	Zeta potential (mV)			
	pI - 0.5	pI - 0.3	pI + 0.3	pI + 0.5
Poly (AA-co-DAC)	8.1 ± 0.9	6.6 ± 0.7	-3.6 ± 1.3	-4.4 ± 1.6
Poly (AA-co-DMC)	5.4 ± 1.2	2.0 ± 1.4	-4.9 ± 0.5	-6.0 ± 2.3
Poly (AA-co-MAPTAC)	11.2 ± 0.9	9.9 ± 1.1	-6.5 ± 1.3	-10.0 ± 1.7
Poly (AA-co-DMAPMA)	11.3 ± 0.6	9.7 ± 0.3	-4.7 ± 1.1	-8.4 ± 1.4
Poly (AA-co-DMAEMA)	4.6 ± 0.4	3.0 ± 1.6	-3.7 ± 1.6	-1.6 ± 0.5

Table 4 Quantum chemical calculations of molecular models of AAPs

Molecular model	ϵ_H (eV)	ϵ_L (eV)	η (eV)	μ (eV)	ω (eV)
Poly (AA-co-DAC)	-0.2804	-0.0185	0.2619	-0.1494	0.0426
Poly (AA-co-DMC)	-0.2805	-0.0223	0.2582	-0.1514	0.0444
Poly (AA-co-MAPTAC)	-0.2671	-0.0099	0.2572	-0.1385	0.0373
Poly (AA-co-DMAPMA)	-0.2243	-0.0014	0.2229	-0.1129	0.0286
Poly (AA-co-DMAEMA)	-0.2183	-0.0092	0.2091	-0.1137	0.0309

their zeta potentials were also higher in the pH range of $pI \pm 0.5$ (Table 3). These data suggested that Poly (AA-co-MAPTAC) and Poly (AA-co-DMAPMA) with amide in the cationic monomers could quickly carry more net charge when the pH climbed over the pI. Therefore, their intra-/inter-chain electrostatic repulsions were rapidly enhanced, which could effectively reduce the degree of aggregation. The results also coincided with the pH dependence and light scattering analysis.

The charge-carrying ability of AAPs was further evaluated by quantum chemical calculations. Lower value of electrophilic factor ω means stronger nucleophilicity and protons binding ability [43–45]. Table 4 shows that the molecular model of Poly (AA-co-MAPTAC) had the

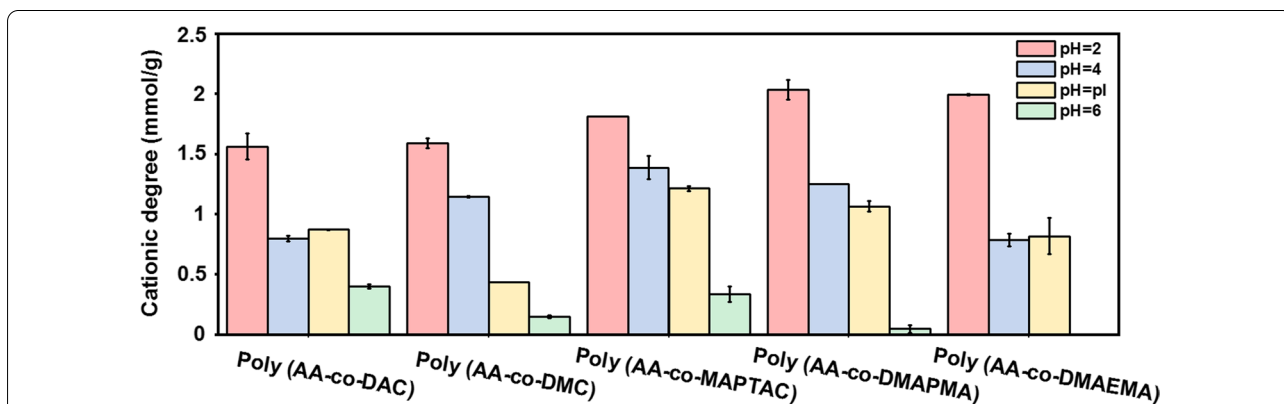


Fig. 5 The cationic degree of AAPs under different pH conditions

lowest ω value of 0.0373 eV among the AAPs with quaternary ammonium groups. For the AAPs with tertiary amine groups, the ω value of the molecular model of Poly (AA-co-DMAPMA) was lower than that of Poly (AA-co-DMAEMA). These results indicated that Poly (AA-co-MAPTAC) and Poly (AA-co-DMAPMA) were easier to bind protons and carry positive charges than the other AAPs, which was consistent with the results in Fig. 5. This should be attributed to the fact that the amide in these two cationic monomers had a stronger electron supplying ability than the ester in the cationic monomers of the other AAPs, and therefore, are convenient in application.

4 Conclusions

Five linear AAPs with similar molecular weights were synthesized using acrylic acid and different cationic monomers. The aggregation of all the AAPs in aqueous solution showed pH and concentration dependence. However, their aggregation behavior was significantly different near the pI. Poly (AA-co-MAPTAC) and Poly (AA-co-DMAPMA) were in the shape of random coils with smaller particle size, while the other AAPs exhibited a hollow spherical shape with more severe aggregation. The reason should be that the amide groups in the cationic monomers (MAPTAC and DMAPMA) enhanced the nucleophilicity of the AAPs, and the corresponding AAPs obtained more positive charges and generated stronger electrostatic repulsion when the pH dropped just below the pI. The results above provide guidance for the design and synthesis of novel amphoteric polymer retanning agent that can maintain a stable solution state over a wide pH range, and therefore, are convenient in application.

Abbreviations

AAP: Amphoteric acrylic polymer; pI: Isoelectric point; AA: Acrylic acid; DAC: Acryloyloxyethyl trimethyl ammonium chloride; DMC: Methacryloxyethyl trimethyl ammonium chloride; MAPTAC: 3-(Methacryloylaminoethyl) trimethyl ammonium chloride; DMAEMA: Dimethylaminoethyl methacrylate; DMAPMA: Dimethylaminopropyl methacrylamide; Poly (AA-co-DAC): Copolymer of AA and DAC; Poly (AA-co-DMC): Copolymer of AA and DMC; Poly (AA-co-MAPTAC): Copolymer of AA and MAPTAC; Poly (AA-co-DMAPMA): Copolymer of AA and DMAPMA; Poly (AA-co-DMAEMA): Copolymer of AA and DMAEMA; DLS/SLS: Dynamic and static light scattering; DWS: Diffusing wave spectroscopy.

Supplementary Information

The online version contains supplementary material available at <https://doi.org/10.1186/s42825-022-00078-3>.

Additional file 1. Fig. S1. FT-IR spectra of Poly (AA-co-DAC) (a), Poly (AA-co-DMC) (b), Poly (AA-co-MAPTAC) (c), Poly (AA-co-DMAPMA) (d) and Poly (AA-co-DMAEMA) (e). **Fig. S2.** ^{13}C -NMR spectra of Poly (AA-co-DAC) (A), Poly (AA-co-DMC) (B), Poly (AA-co-MAPTAC) (C), Poly (AA-co-DMAPMA) (D) and Poly (AA-co-DMAEMA) (E).

Acknowledgements

We thank Dr. Bin Liu from Nanjing Tech University and Dr. Pengfei Sun from Nanjing University of Posts and Telecommunications for guiding DLS/SLS measurements, and thank Prof. Wenhua Zhang from National Engineering Laboratory for Clean Technology of Leather Manufacture, Sichuan University for guiding quantum chemical calculations.

Authors' contributions

QL, JL, and YW conceived the idea. QL performed the experiments and drafted the manuscript. YY participated in part of the experiments. YW and BS analyzed the results and revised the manuscript. All authors read and approved the final manuscript.

Funding

This work was financially supported by the Tianfu Ten-thousand Talents Program of Sichuan Province and the National Key R&D Program (2017YFB0308500).

Availability of data and materials

All data from this study are presented in the paper and the additional file.

Declarations

Competing interests

The authors declare that they have no competing interests.

Author details

¹Key Laboratory of Leather Chemistry and Engineering (Sichuan University), Ministry of Education, Chengdu 610065, China. ²National Engineering Laboratory for Clean Technology of Leather Manufacture, Sichuan University, Chengdu 610065, China. ³Sichuan Tingjiang New Material, Inc., Shifang 618412, China.

Received: 8 November 2021 Accepted: 20 January 2022

Published online: 15 February 2022

References

1. Yu Y, Lin YR, Zeng YH, Wang YN, Zhang WH, Zhou JF, et al. Life cycle assessment for chrome tanning, chrome-free metal tanning, and metal-free tanning systems. *ACS Sustain Chem Eng*. 2021;9(19):6720–31. <https://doi.org/10.1021/acssuschemeng.1c00753>.
2. Wang YN, Shi B. Progress of key clean technologies in leather industry. *Chem Ind Eng Prog*. 2016;35(6):1865–74. <https://doi.org/10.16085/j.issn.1000-6613.2016.06.028>.
3. Hedberg YS. Chromium and leather: a review on the chemistry of relevance for allergic contact dermatitis to chromium. *J Leath Sci Eng*. 2020;2(1):1–15. <https://doi.org/10.1186/s42825-020-00027-y>.
4. Yu Y, Wang YN, Ding W, Zhou JF, Shi B. Preparation of highly-oxidized starch using hydrogen peroxide and its application as a novel ligand for zirconium tanning of leather. *Carbohydr Polym*. 2017;174:823–9. <https://doi.org/10.1016/j.carbpol.2017.06.114>.
5. Guo XR, Yu Y, Wang YN, Shi B. Oxidized maltodextrin: a novel ligand for aluminum–zirconium complex tanning. *J Am Leather Chem As*. 2021;116(5):155–61. <https://doi.org/10.34314/jalca.v116i5.4293>.
6. Wang YN, Huang WL, Zhang HS, Tian L, Zhou JF, Shi B. Surface charge and isoelectric point of leather—a novel determination method and its application in leather making. *J Am Leather Chem As*. 2017;112(7):224–31.
7. Song Y, Wang YN, Zeng YH, Wu HP, Shi B. Quantitative determinations of isoelectric point of retanned leather and distribution of retanning agent. *J Am Leather Chem As*. 2018;113(7):232–8.
8. Huang WL, Song Y, Yu Y, Wang YN, Shi B. Interaction between retanning agents and wet white tanned by a novel bimetal complex tanning agent. *J Leath Sci Eng*. 2020;2(1):1–9. <https://doi.org/10.1186/s42825-020-00023-2>.
9. Wang XC, Wang WN, Liu XH, Wang YY. Amphoteric functional polymers for leather wet finishing auxiliaries: a review. *Polym Advan Technol*. 2021;32(5):1951–64. <https://doi.org/10.1002/pat.5248>.

10. Wang XC, Sun SW, Zhu X, Guo PY, Liu XH, Liu CL, Lei M. Application of amphoteric polymers in the process of leather post-tanning. *J Leath Sci Eng*. 2021;3(1):1–9. <https://doi.org/10.1186/s42825-021-00050-7>.
11. Hao DY, Wang XC, Liu XH, Zhu X, Sun SW, Li J, Yue OY. A novel eco-friendly imidazole ionic liquids based amphoteric polymers for high performance fatliquoring in chromium-free tanned leather production. *J Hazard Mater*. 2020;399:123048. <https://doi.org/10.1016/j.jhazmat.2020.123048>.
12. Ma JZ, Liu QW, Wu MX, Tian ZH. Preparation and assistant-dyeing of formaldehyde-free amphoteric acrylic retanning agent. *J Leath Sci Eng*. 2021;3(1):1–13. <https://doi.org/10.1186/s42825-021-00066-z>.
13. Wang XC, Hao DY, Chai XY, Li J. Effect of an amphoteric chromium-free polymer retanning agent with reactive aldehyde groups on collagen fibers. *J Am Leather Chem As*. 2019;114(10):373–81.
14. Xu W, Chai XY, Zhao GH, Li J, Wang XC. Preparation of reactive amphoteric polyurethane with multialdehyde groups and its use as a retanning agent for chrome-free tanned leather. *J Appl Polym Sci*. 2019;136(37):47940. <https://doi.org/10.1002/app.47940>.
15. Wang XC, Yan Z, Liu XH, Qiang TT, Chen LA, Guo PY, Yue OY. An environmental polyurethane retanning agent with the function of reducing free formaldehyde in leather. *J Clean Prod*. 2019;207:679–88. <https://doi.org/10.1016/j.jclepro.2018.10.056>.
16. Xu W, Yang R, Chai XY, Qiang XH, Wang XC, Zhao T. Preparation and application of amphoteric phenolic synthetic tanning agent. *China Leather*. 2021;50(6):19–24. <https://doi.org/10.13536/j.cnki.issn1001-6813.2021-006-004>.
17. Gohy JF, Creutz S, Garcia M, Mahltig B, Stamm M, Jerome R. Aggregates formed by amphoteric diblock copolymers in water. *Macromolecules*. 2000;33(17):6378–87. <https://doi.org/10.1021/ma992016j>.
18. Song J, Yamaguchi T, Silva DJ, Hubbe MA, Rojas OJ. Effect of charge asymmetry on adsorption and phase separation of polyampholytes on silica and cellulose surfaces. *J Phys Chem B*. 2010;114(2):719–27. <https://doi.org/10.1021/jp909047t>.
19. Rabiee A, Ershad-Langroudi A, Jamshidi H. Polyacrylamide-based polyampholytes and their applications. *Rev Chem Eng*. 2014;30(5):501–19. <https://doi.org/10.1515/revce-2014-0004>.
20. Higgs PG, Joanny JF. Theory of polyampholyte solutions. *J Chem Phys*. 1991;94(2):1543–54.
21. Chen FS, Xie LS, Wei DJ, Chen XY. Determination of the charge of polymers by colloidal titration. *China Pap*. 2000;2:30–4.
22. Plank J, Sachsenhauser B. Experimental determination of the effective anionic charge density of polycarboxylate superplasticizers in cement pore solution. *Cem Concr Res*. 2009;39(1):1–5. <https://doi.org/10.1016/j.cemconres.2008.09.001>.
23. Das I, Borah JH, Sarma D, Hazarika S. Synthesis of PAMAM dendrimer and its derivative PAMOL: determination of thermophysical properties by DFT. *J Macromol Sci A*. 2018;55(7):544–51. <https://doi.org/10.1080/10601325.2018.1481345>.
24. Esmkhani R, Monajjemi M. Electronic structural investigation of boron nitride nano cage ($B_{30}N_{20}$) in point of exchange and correlation energy. *J Comput Theor Nanos*. 2015;12(4):652–9. <https://doi.org/10.1166/jctn.2015.3782>.
25. Zhang YK, Yang W. Perspective on “Density-functional theory for fractional particle number: derivative discontinuities of the energy.” *Theor Chem Acc*. 2000;103:346–8. https://doi.org/10.1007/978-3-662-10421-7_57.
26. Chen Y, Feng L, Liu BZ, Peng JL, Chen Y, Xu CA, Ren J. Study of microwave-template initiated copolymerization peculiarity and evaluation on the coal floc distinctive behavior and flocculation performance. *J Appl Polym Sci*. 2020;137(46):49519. <https://doi.org/10.1002/app.49519>.
27. Harn YW, He YJ, Wang ZW, Chen YH, Liang S, Li ZL, Li Q, Zhu L, Lin ZQ. Synthesis of amphiphilic and double hydrophilic star-like block copolymers and the dual pH-responsiveness of unimolecular micelle. *Macromolecules*. 2020;53(19):8286–95. <https://doi.org/10.1021/acs.macromol.0c00918>.
28. Yang JJ, Li J, Tang BT, Zhang SF. Solution properties of amphoteric macromolecular dyes derived from poly (acrylamide-co-vinylamine). *J Polym Res*. 2015;22(2):1–8. <https://doi.org/10.1007/s10965-015-0659-9>.
29. Dong AJ, Hou GL, Wang YX, Sun DX. Properties of amphoteric polyurethane waterborne dispersions. I. Dependence on pH value in salt-free media. *J Polym Sci Pol Phys*. 2002;40(10):972–9. <https://doi.org/10.1002/polb.10153>.
30. Kamiyama Y, Israelachvili J. Effect of pH and salt on the adsorption and interactions of an amphoteric polyelectrolyte. *Macromolecules*. 1992;25(19):5081–8. <https://doi.org/10.1021/ma00045a039>.
31. Xu SM, Wu RL, Huang XJ, Gao LQ, Wang JD. Effect of the anionic-group/cationic-group ratio on the swelling behavior and controlled release of agrochemicals of the amphoteric, superabsorbent polymer poly (acrylic acid-co-diallyldimethylammonium chloride). *J Appl Polym Sci*. 2006;102(2):986–91. <https://doi.org/10.1002/app.23990>.
32. Armentrout RS, McCormick CL. Water-soluble polymers. 77. Amphoteric cyclopolymers with sulfobetaine units: Phase behavior in aqueous media and solubilization of p-cresol in microdomains. *Macromolecules*. 2000;33(8):2944–51. <https://doi.org/10.1021/ma991531e>.
33. Mincheva R, Bougard F, Paneva D, Vachaudéz M, Manolova N, Dubois P, Rashkov I. Self-assembly of N-carboxyethylchitosan near the isoelectric point. *J Polym Sci Pol Chem*. 2008;46(20):6712–21. <https://doi.org/10.1002/pola.22978>.
34. Sletmoen M, Geissler E, Stokke BT. Determination of molecular parameters of linear and circular scleroglucan coexisting in ternary mixtures using light scattering. *Biomacromol*. 2006;7(3):858–65. <https://doi.org/10.1021/bm050990m>.
35. Li LW, He C, He WD, Wu C. Formation kinetics and scaling of “defect-free” hyperbranched polystyrene chains with uniform subchains prepared from seasaw-type macromonomers. *Macromolecules*. 2011;44(20):8195–206. <https://doi.org/10.1021/ma201687s>.
36. Xie D, Jiang M, Zhang GZ, Chen DY. Hydrogen-bonded dendronized polymers and their self-assembly in solution. *Chem Eur J*. 2007;13(12):3346–53. <https://doi.org/10.1002/chem.200601361>.
37. Gasilova ER, Lapina IM, Kulminskaya AA, Skorik YA. Branched architecture of fucoidan characterized by dynamic and static light scattering. *Colloid Polym Sci*. 2020;298(10):1349–59. <https://doi.org/10.1007/s00396-020-04706-4>.
38. Maia AMS, Costa M, Borsali R, Garcia RB. Rheological behavior and scattering studies of acrylamide-based copolymer solutions. *Macromol Symp*. 2005;229(1):217–27. <https://doi.org/10.1002/masy.200551127>.
39. Xu JY, Boddu VM, Liu SX, Liu WC. A comparative study of microrheology of nanocellulose produced from corn stover using diffusing wave spectroscopy (DWS) and mechanical rheometry. *Cell Chem Technol*. 2020;54(1–2):27–32. <https://doi.org/10.35812/CelluloseChemTechnol.2020.54.03>.
40. Scheffold F. Particle sizing with diffusing wave spectroscopy. *J Disper Sci Technol*. 2002;23(5):591–9. <https://doi.org/10.1081/DIS-120015365>.
41. Niu F, Ahmad M, Fan JM, Ritzoulis C, Chen JS, Luo ZS, Pan WC. The application of diffusing wave spectroscopy (DWS) in soft foods. *Food Hydrocolloids*. 2019;96:671–80. <https://doi.org/10.1016/j.foodhyd.2019.06.011>.
42. Xu JY, Inglett GE, Liu SX, Boddu VM. Micro-heterogeneity and micro-rheological properties of high-viscosity barley β -glucan solutions studied by diffusing wave spectroscopy (DWS). *Food Biophys*. 2016;11(4):339–44. <https://doi.org/10.1007/s11483-016-9447-2>.
43. Parr RG, Szentpály L, Liu S. Electrophilicity index. *J Am Chem Soc*. 1999;121(9):1922–4. <https://doi.org/10.1021/ja983494x>.
44. Ayers PW, Parr RG, Pearson RG. Elucidating the hard/soft acid/base principle: a perspective based on half-reactions. *J Chem Phys*. 2006;124(19):194107. <https://doi.org/10.1063/1.2196882>.
45. Pérez P. Global and local electrophilicity patterns of diazonium ions and their reactivity toward π -nucleophiles. *J Org Chem*. 2003;68(15):5886–9. <https://doi.org/10.1021/jo030125x>.

Publisher's Note

Springer Nature remains neutral with regard to jurisdictional claims in published maps and institutional affiliations.